Drug loaded homogeneous electrospun PCL/gelatin hybrid nanofiber structures for anti-infective tissue regeneration membranes

Jiajia Xue [a], Min He [a], Hao Liu [b], Yuzhao Niu [a], Aileen Crawford [c], Phil Coates [d], Dafu Chen [e], Rui Shi [e,*], Liqun Zhang [a,*]

[a]Beijing Laboratory of Biomedical Materials, Beijing University of Chemical Technology, Beijing 100029, China

[b]DaBeiNong Group (DBN) Research Center for Animal Medicine, Beijing 100195, PR China

[c]Centre for Biomaterials and Tissue Engineering, University of Sheffield, Sheffield, South Yorkshire S3 7HQ, UK

[d]School of Engineering, Design & Technology, University of Bradford, Bradford, West Yorkshire BD7 1DP, UK

[e]Laboratory of Bone Tissue Engineering of Beijing Research Institute of Traumatology and Orthopaedics, Beijing 100035, China.

*Corresponding authors.

1. Beijing Laboratory of Biomedical Materials, Beijing University of Chemical Technology, Beijing 100029, PR China. Tel.:+86 10 64421186; fax: +86 10 64433964.

   E-mail address: zhanglq@mail.buct.edu.cn (L. Zhang).

2. Laboratory of Bone Tissue Engineering of Beijing Research Institute of Traumatology and Orthopaedics, Beijing 100035, China.

   Email address: sharell@126.com (R. Shi).

Abstract

Infection is the major reason for guided tissue regeneration/guided bone regeneration (GTR/GBR) membrane failure in clinical application. In this work, we developed GTR/GBR membranes with localized drug delivery function to prevent infection by electrospinning of poly(ε-caprolactone) (PCL) and gelatin blended with metronidazole (MNA). Acetic acid (HAc) was introduced to improve the miscibility of PCL and gelatin to fabricate homogeneous hybrid nanofiber membranes. The effects of the addition of HAc and the MNA content (0, 1, 5, 10, 20, 30, and 40 wt.% of polymer) on the properties of the membranes were investigated. The membranes showed good mechanical properties, appropriate biodegradation rate and barrier function. The controlled and sustained release of MNA from the membranes significantly prevented the colonization of anaerobic bacteria. Cells could adhere to and proliferate on the membranes without cytotoxicity until the MNA content reached 30%. Subcutaneous implantation in rabbits for 8 months demonstrated that MNA-loaded membranes evoked a less severe inflammatory response depending on the dose of MNA than bare membranes. The biodegradation time of the membranes was appropriate for tissue regeneration. These results indicated the potential for using MNA-loaded PCL/gelatin electrospun membranes as anti-infective GTR/GBR membranes to optimize clinical application of GTR/GBR strategies.

Keywords:

Guided tissue regeneration; Anti-infection; Electrospinning; Drug delivery

Introduction

Guided tissue regeneration/guided bone regeneration (GTR/GBR) technologies are a frequently used standard procedure for tissue and bone regeneration therapy [1]. The principle of GTR/GBR membranes is used not only to perform the barrier function by preventing the ingrowth of fibroblast cells into the tissue/bone defect site but also to improve the tissue/bone regeneration by supporting cells to attach and proliferate [2].Conventionally, GTR/GBR membranes require flexibility to adapt to and optimally cover a tissue defect, biocompatibility, and proper degradation profile to eliminate the need for membrane removal surgery [3].

Infection is currently considered as the major reason for GTR/GBR failure in clinical applications, constituting a significant healthcare burden [4]. Infection is caused by either bacterial colonization at the wound site or foreign body response resulting from the implant material [5].Antibacterial biomaterials are one of the greatest interests in the war against implant-related infections, representing the broadest group of anti-infective biomaterials [6]. Focal antibacterial drug-loaded biomaterials can deliver a desired drug dose directly to the infected site for an extended time period while minimizing systemic distribution of toxic drugs [7,8]. Infection associated with GTR/GBR implant is mainly caused by anaerobic bacteria [9,10]. Metronidazole (MNA), which has selective activity against anaerobic microorganisms including bacteria and protozoa [11], has been successfully used for the treatment of anaerobic bacterial infections for more than 45 years [12]. MNA-loaded poly(lactic-co-glycolic acid) membrane fabricated by solvent casting showed a significant improvement on the periodontal regeneration following GTR in dogs [13].Our purpose is to develop an anti-infective GTR/GBR membrane with sufficient localized MNA release.

Electrospinning has gained widespread interest in tissue engineering and drug delivery because of its relative ease of use and adaptability [14]. The inherently high surface to volume ratio of electrospun polymer fibers can improve cell attachment, enhance drug loading, and realize sustained and controlled local drug delivery [15]. The drug release profile and the degradation rate of the electrospun membranes can be adjusted by regulating the

electrospinning parameters [16]. Therefore, electrospinning was adopted to fabricate the antibacterial membranes in this study.

Numerous natural and synthetic polymers have been investigated for the fabrication of GTR/GBR membranes. Collagen has excellent biocompatibility, but it collapses quickly during the degradation process [17]. Although poly(lactic acid)- and poly(lactic-co-glycolic acid)-based nanofiber membranes are also non-cytotoxic and biodegradable, the rapid releases of oligomers and acid by-products during degradation may cause significant inflammation reactions and foreign body response in vivo [18]. PCL is extensively studied for controlled drug delivery because of its compatibility with a wide range of drugs and good mechanical properties [19,20],but it often results in low cell adhesion and proliferation and the biodegradation rate of PCL is low. Gelatin, a natural biopolymer derived from partial hydrolysis of native collagen, has many integrin-binding sites for cell adhesion and differentiation [21]. PCL-gelatin hybrid material, a new biomaterial with good biocompatibility and improved mechanical, physical, and chemical properties [22], has been successfully used in various tissue engineering applications [23-25]. However, phase separation between PCL and gelatin adversely affect both the electrospinning process and the resultant fiber performance. Induction of acetic acid was reported to be effective in mediating the miscibility of PCL and gelatin and forming homogeneous nanofibers with improved performance [26].

On the basis of the aforementioned, MNA-loaded homogeneous PCL/gelatin electrospun nanofiber membranes were fabricated. The current study aimed to (i) develop MNA-loaded membranes as anti-infective GTR/GBR membranes and (ii) investigate their anti-bacterial and anti-infection properties by using a long term subcutaneous implantation model. For these purposes, GTR/GBR membranes were prepared by blending PCL, gelatin, and MNA by using an electrospinning technique. HAc was added to the electrospinning system to obtain homogeneous nanofibers. Our hypothesis was that (i) the electrospun membranes containing the use of HAc would show improved performance and (ii) the electrospun PCL/gelatin membrane loaded with MNA would reduce bacterial

colonization and hence prevent infection in the defect site. The current work is expected to provide valuable information for the development of anti-infective GTR/GBR membranes.

2. Materials and methods

2.1. Materials

PCL (M_n=70-90 kDa) and 3-(4,5-dimethylthiazol-2-yl)-2,5-diphenyltetrazolium bromide (MTT) were purchased from Sigma-Aldrich (St. Louis, USA) and used as received. Gelatin was purchased from Rousselot (France). Metronidazole (MNA) was purchased from Tokyo Chemical Industry Co., Ltd. (Japan). Dulbecco's modified eagle medium (DMEM), fetal bovine serum (FBS), 0.05% Trypsin EDTA, and phosphate buffer saline (PBS, pH=7.4) were purchased from Gibco (USA). Methanol and trifluoroethanol (TFE) were purchased from Alfa-Aesar Chemical Inc. (USA). WST-8, polyformaldehyde and FITC–phalloidin were purchased from Beyotime Institute of Biotechnology (China). Other chemical reagents such as acetic acid, dichloromethane (DCM), and N-N'dimethylformamide (DMF) were purchased from Sinopharm Chemical Reagent Beijing Co., Ltd. (China) and used without further purification. MGC AnaeroPack™ Series was purchased from Mitsubishi Gas Chemical Company, Inc. (Japan). Brain heart infusion (BHI) broth and BHI agar were purchased form Oxoid (UK). L929 fibroblast cell lines were kindly donated by Jishuitan Hospital. Human periodontal ligament fibroblasts (hPDLFs) and rat osteogenesis sample (ROS) cells were kindly donated by University of Sheffield (UK).

2.2. Electrospinning nanofiber membranes

A solution of PCL-gelatin was prepared by mixing 6 wt.% PCL/TFE and 6 wt.% gelatin/TFE in the mass ratio of 50:50. A tiny amount (0.2 v/v% TFE) of HAc was dropped to the solution to obtain a transparent PCL-gelatin-HAc (PGH) solution. MNA in the range of 1-40 wt.% of the polymer used was added to the PGH solution. The solution was fed at a rate of 1 mL/h by a syringe pump to the needle tip of a 20 mL syringe. Optimized high voltage (8-12 kV) was applied between the needle and the grounded collector, which was laid with aluminum foil at a rotating

rate of 300 rpm. The needle was located at a distance of 20 cm from the ground collector. The membranes with MNA contents of 1%, 5%, 10%, 20%, 30%, and 40% were labeled as PGH1, PGH5, PGH10, PGH20, PGH30, and PGH40, respectively. To investigate the influence of incorporated gelatin and HAc on the properties of PGH-MNA membranes, membranes electrospun from PCL-MNA solution and PCL-gelatin-MNA solution were fabricated as control and labeled as Pc and PGc (c is the MNA content) , respectively.

2.3. Characterization of PGH-MNA nanofiber membranes

2.3.1. Morphology

The morphology of the membranes was observed by scanning electron microscopy (SEM). The fiber diameter and pore size were measured by using the Image J software on SEM micrographs at 100 random locations. The thickness of a membrane was measured with a micrometer. The apparent density and porosity of the membrane were calculated by using equations (1) and (2), respectively [27]:

$$\text{Apparent density } (\text{g}/cm^3) = \frac{\text{Mass of membrane (g)}}{\text{Membrane thickness (cm)} \times \text{Membrane area (cm}^2\text{)}}, \quad (1)$$

$$\text{Porosity } (\%) = \left(1 - \frac{\text{Apparent density } (\text{g}/cm^3)}{\text{Bulk density } (\text{g}/cm^3)}\right) \times 100\% \quad (2)$$

2.3.2. Molecular dynamics simulation, chemical, thermal, and mechanical analyses

The interaction between PCL and MNA was investigated by molecular dynamics simulation (see S1). Fourier transform infrared (FT-IR) spectra were performed on a Bruker Tensor 27 spectrometer. The scan range was 4000 cm^{-1} to 600 cm^{-1} with a resolution of 2 cm^{-1}. Differential scanning calorimetry (DSC) measurements were performed with a Mettler-Toledo DSC instrument under nitrogen. The measurements were carried out at cooling and heating rate of 10 ℃/min from –100 ℃ to 220 ℃. X-ray diffraction (XRD) studies were conducted on a Rigaku D/max-Ultima III X-ray diffractometer equipped with Cu-K α source (40 kV, 40 mA) in the range of 5 °to 50 °at a scan rate of 5 °/min.

The tensile properties of the membranes in both the dry state and the wet state were evaluated by using a BOSE

ElectroForce 3200 test instrument with a 50-N load cell at a crosshead speed of 5 mm/min at the ambient temperature of 25 °C. All samples were cut into rectangles with dimensions of 25 mm×4 mm. Five samples in the dry state were tested for each membrane. Another five samples were soaked in deionized water for 1 h for wet state measurements. The thicknesses of the samples were measured with a micrometer accurate to 1 μm.

2.3.3. Apparent water contact angle (WCA) measurements

The static WCA of a membrane was measured by a SL200A type Contact Angle Analyzer (Solon (Shanghai) Technology Science Co., Ltd., China) at ambient temperature. Water droplets (3.0 μL) were dropped carefully onto the surface of the membrane. The average WCA value was obtained by measuring ten water droplets at randomly distributed positions.

2.3.4. Drug encapsulation efficiency and drug release profile

The drug encapsulation efficiency was determined as follows. A known mass of membrane was dissolved in 1 mL of TFE, and the solution was added dropwise to 20 mL of methanol, in which the polymer was precipitated and MNA was dissolved. After centrifugation of the methanol solution, the liquid supernatant was detected by High Performance Liquid Chromatography (HPLC) at λ_{max} =310 nm. The amount of MNA was obtained from the calibration curve of MNA. The encapsulation efficiency was calculated by the following equation:

$$\text{Encapsulation efficiency } \% = \frac{\text{weight of drug in the sample (g)}}{\text{theoretical weight of drug loading in the sample (g)}} \times 100\% \qquad (3).$$

The drug release profile was determined by soaking the membrane in triplicate in PBS. The membrane was cut into circles 2 cm in diameter, accurately weighed, and incubated in 5 mL of PBS at 37 °C with mild shaking. At pre-determined time intervals, 1 mL of soaking solution was collected for HPLC detection to determine the amount of drug released. The remaining medium was removed and replaced with another 5 mL of fresh PBS to maintain the sink condition. The percentage of the drug released was calculated based on the initial weight of the drug

incorporated in the electrospun membrane.

2.3.5. In vitro biodegradation

The membrane was cut into circular samples 2 cm in diameter, weighed, and soaked in 5 mL of PBS in 12-well plates at 37 ºC. Samples were carefully removed from the wells at predetermined times, rinsed with Milli-Q water for three times, dried at 50 ºC until the weight underwent no further changes, and then weighed. The sample weights were plotted against time to obtain the degradation profile of the membrane. The morphology and tensile properties of the membrane during degradation were measured by SEM and tensile testing, respectively.

2.4. Barrier function, antibacterial activity, and biocompatibility

2.4.1. Barrier function to fibroblast cells

The *in vitro* barrier function of the membranes to L929 cells as model cells was evaluated by an elegant method we designed (schematic diagram as shown in S2). Each membrane was cut into a circle 2.5 cm in diameter, sterilized, fixed on a CellCrown™ (Sigma, USA), and put into a 24-well plate without touching the bottom of the well. L929 cells were resuspended in DMEM supplemented with 10% (v/v) FBS at a density of 4.0×10^4 cells/mL. Then 1 mL of culture medium without cells was added to the well from the outside of the CellCrown™, and 900 μL of culture medium plus 100 μL of cell resuspension was added onto the sample. After incubated at 37 ºC under a 5% CO_2 atmosphere for 1 day, 3 days, 5 days, and 7 days, the CellCrown™ was taken out, and the bottom of the 24-well plate was observed under an inverted phase contrast microscope (Olympus IX50-S8F2) to determine whether the cells got through the membrane to the bottom of the well or the culture medium. The other side of the membrane, which had no contact with the cells, was observed under a scanning electron microscope to find out whether the cells penetrated the membrane. The barrier function of the membranes after 1 month of degradation in PBS was also evaluated as above.

2.4.2. In vitro antibacterial activity

The antibacterial activity of the membranes against the typical anaerobic bacterium Fusobacterium nucleatum (ATCC 25586, Chinese General Microbiological Culture Collection Center), which is commonly found in the oral cavity in an infection [28], was determined by the modified Kirby–Bauer method [29] under anaerobic conditions [30]. Anaerobic environment was created by using MGC AnaeroPack™-Anaero Series (Anaero-2.5 L is a disposable oxygen-absorbing and carbon dioxide generating agent for use in anaerobic jars, which has been widely used in laboratories to create anaerobic environment). The bacterial strain was inoculated onto BHI agar and anaerobically incubated at 37 ℃ for 24 h. After incubation, isolated bacterial colonies of the stock culture were suspended in sterile BHI broth until the turbidity was compatible with 0.5 Mac Farland. A 100 μL Fusobacterium nucleatum suspension was spreaded onto a BHI agar plate. Samples (1.0 cm×1.0 cm) of a membrane in triplicate were pasted onto the agar plate and incubated anaerobically for different times at 37 °C. All the samples were sterilized for 3 h under UV before they were pasted. The bacterial growth on the plate was visualized directly, after anaerobic incubation of the plates at 37 ℃ for 48 h, the diameter of the inhibition zone was measured.

2.4.3. Cytotoxicity and proliferation of cells on the membranes

The cytotoxicity of the membranes to L929 fibroblast cells, hPDLFs, and ROS cells was evaluated (see S3). The viabilities of L929 cells proliferated on the membranes were assessed by using CCK-8 assay referred to the manufacturer's protocol. The membrane was cut into circles 2.5 cm in diameter and sterilized, then fixed in the well of a 24-well plate by Cell-Crown™. L929 cells were resuspended in DMEM supplemented with 10% FBS and antibiotics (100 μg/mL penicillin and 100 mg/mL streptomycin) at a density of 4.0×10^4 cells/mL. Cell culture medium (800 μL) and cell resuspension (100 μL) were plated onto the sample carefully. Cell resuspensions added into wells with no samples were regarded as control. Plates were incubated at 37 °C under 5% CO_2 atmosphere. The medium was changed every two days. At days 1, 3, 5, and 7 of culture, the sample was washed with PBS for three times to remove the cells that did not attach to the membrane, and 100 μL of WST-8 (final dilution: 1:10),

which can react with dehydrogenase in mitochondria to form a water soluble formazan, was added onto the sample to test the live cells. Then 100 μL of supernatants was transferred into a 96-well plate for optical density (O.D.) measurements at 450 nm. The cell-cultured membrane was afterwards washed with PBS for three times, fixed with 3% glutaraldehyde at 4 ^{o}C for 2 h, soaked in 0.18 M sucrose solutions at 4 ^{o}C for 2 h, dehydrated through a series of graded ethanol solutions, and lyophilized overnight. The morphologies of the cells on the membranes were observed by using SEM.

The morphologies of the cells were also observed using laser scanning confocal microscope (CLSM, Olympus, FV1000-IX81). After incubated for 3 days and 7 days, the cell-cultured samples were washed twice with PBS, fixed with 4% polyformaldehyde for 10 min, and then stained with FITC–phalloidin solution (5 μg/mL) for 1 h. The samples were washed three times with PBS and visualized with CLSM. The CLSM images were obtained by focusing on the surface of the membranes as z-position.

The proliferation of hPDLFs and ROS cells on the membranes were also tested by PrestoBlue assay. The membranes cut into circles 2.5 cm in diameter were disinfected in 100% isopropanol for 20 minutes and then rinsed in PBS for three times. The circular samples were fixed with Cell-Crown^{TM} on a 24-well plate. After the addition of 800 μL of culture medium on the membrane per well, hPDLFs and ROS cells separately resuspended in 100 μL of culture medium at a density of 5×10^{5} cells/mL were added gently on each membrane. After 2 days of incubation, 100 μL of PrestoBlue^{TM} was pipetted per well. At 1 hour incubation, 200 μL of supernatants was transferred into a 96-well plate, and fluorescence intensity was measured using a fluorescence reader (TECAN Spectrophometer) at an excitation wavelength of 570 nm and emission wavelength of 600 nm.

2.5. In vivo biocompatibility and biodegradation

To evaluate the influence of MNA content on the *in vivo* anti-infection property, biocompatibility, and biodegradability of the membranes, PGH5, PGH10, and PGH30 were subcutaneous implanted while P0 and P30

were used as control.

Forty healthy adult male New Zealand white rabbits (2.5–3.0 kg each) were used as experimental animals. The protocol for animal experiments was approved by the Animal Ethical Committee of the Laboratory of Bone Tissue Engineering of Beijing Research Institute of Traumatology and Orthopedics, and national guidelines for the care and use of laboratory animals were applied. Samples (1.5 cm×1.5 cm) were sterilized by γ-irradiation. The animals were anesthetized with isoflurane, and their backs were shaved and sterilized with alcohol and iodine scrubs. Three paravertebral incisions (2 cm each) per rabbit were made approximately 1 cm lateral to the vertebral column to expose the dorsal subcutis. Subcutaneous pockets were created by blunt dissection. Each individual pocket held one membrane, and the incisions were closed with surgical sutures. All surgeries were carried out in an aseptic field by using aseptic technique. The long term biocompatibility of the samples was evaluated for 8 months of implantation [25,26]. After post-surgery 1 week, 3 weeks, 5 weeks, 7 weeks, 8 weeks, 3 months, 6 months, and 8 months, the implants were harvested and stained with hematoxylin and eosin (H&E) for morphological evaluation as usual procedure. The infiltration of inflammatory cells and the thickness of the inflammatory fibrous capsule formed around a cross section of the implant were assessed to evaluate the extent of inflammation, foreign body reaction and biocompatibility of each sample. Explanted membranes were observed by SEM.

2.6. Statistical analysis

Statistical comparisons for significance were conducted using Students' t-test with a 95% confidence level. Each data point was expressed as mean ± standard deviation.

3. Results

3.1. Characterization of electrospun membranes

3.1.1. Influence of HAc on morphology of PCL-gelatin electrospun membranes

Because of the sol-gel transition of gelatin and the immiscibility of PCL and gelatin, the mixed solution of

PCL/TFE and gelatin/TFE becomes opaque and gradually separates into different layers after being mixed for 3 hours. After a tiny amount of HAc was added to the mixed solution, the pH of the solution is away from the isoelectric point of gelatin, restricting the sol-gel transition of gelatin. Besides, the gelatin molecules, which are positively charged because of the protonation of amino groups, become mutually exclusive and entangle with the PCL chains [18].A miscible and transparent solution was formed and no sign of two liquid layers was observed, as shown in Fig. S3. Micro- and nanofibers coexist in PG0 while smooth and uniform nanofibers are exclusively formed in PGH0. The hierarchically sized fibers of PG0 will influence the overall homogeneity of the membranes.

3.1.2. Morphology of electrospun membranes

The SEM micrographs of the PGH-MNA membranes (Fig. 1) show a randomly interconnected structure with no beads formed and uniform distribution of nanofibers. As shown in Table 1, the diameters of the nanofibers are influenced by the MNA content, the nanofibers of PGH10 being the thinnest. The much smaller pore sizes of the membranes than the size of fibroblasts are beneficial to preventing the ingrowth of fibroblasts into the tissue defects. The porosities of the membranes are all in the range of 60%-80%, ensuring sufficient gas and nutrient exchanges. Thus, we have successfully fabricated drug-loaded homogeneous hybrid nanofiber membranes.

3.1.3. Chemical, thermal, and mechanical properties and hydrophilicity of the nanofiber membranes

The compatibility and interaction between the polymer matrix and drug influence the encapsulation and release of drugs in the nanofibers [18].Molecular dynamics simulation results showed that MNA can form hydrogen bonds (HBs) with PCL (S4) while the MNA molecules, which are hydrophilic, also have interaction with gelatin.

According to the ATR-FTIR spectra of the electrospun membranes (Fig. 2A), the characteristic peaks of gelatin appear at approximately 1650 cm^{-1} (amide I) and 1540 cm^{-1} (amide II). The PCL-related stretching modes are represented by the peaks at 2943 cm^{-1} (asymmetric CH_2 stretching), 2866 cm^{-1} (symmetric CH_2 stretching), 1721 cm^{-1} (C=O stretching), 1294 cm^{-1} (C-O and C-C stretching), and 1240 cm^{-1} (asymmetric C-O-C stretching) [31].

The MNA-related stretching modes represented by the peaks at 3414 cm^{-1} and 3220 cm^{-1} (O-H stretching), 3097 cm^{-1} (=CH stretching), and 1550 cm^{-1} (-NO_2 antisymmetric stretching), are no different from those of pure MNA crystals. The relative intensities of these peaks increase with increasing MNA content. Besides, the width of the characteristic hydroxyl peaks of MNA at 3414 cm^{-1} and 3220 cm^{-1} increase compared with that of pure MNA, because of the hydrogen interaction between MNA and the polymer matrix. Other interactions include the hydrogen interaction between PCL and gelatin [31]. By adding HAc, the chain entanglement and hydrogen interaction between PCL and gelatin increase, and MNA disperses more homogenously in the electrospinning solution. The electrospinning process does not adversely affect the molecular structure of MNA, especially the antibacterial -NO_2 group.

The DSC thermograms of the membranes are shown in Fig. 2B. At MNA contents lower than 20%, the absence of the MNA melting peak indicates that MNA is dispersed on the molecular level. At MNA contents of 20%, 30%, and 40%, the melting peak of MNA appears, indicating the formation of MNA crystals. The endothermic enthalpy of melting of a perfect PCL crystal is 139 J/g [32], and the endothermic melting enthalpies of PCL in P0, PG0, and PGH0 are 70.4 J/g, 68.1 J/g, and 66.0 J/g, respectively. From these enthalpy data, the degrees of crystallinity of PCL in P0, PG0, and PGH0 are calculated to be 50.6%, 49.0%, and 47.5%, respectively. The crystallinity of PCL decreases with the incorporation of gelatin and HAc. With the incorporation of gelatin, the gelatin molecular chains entangle with PCL molecular chains. With the further addition of HAc, the miscibility and interaction between gelatin and PCL are improved, resulting in more chain entanglements, which restrict the chain mobility and crystallization of PCL. The lower crystallinity of PCL indicates better miscibility of PCL and gelatin hybrid nanofibers. For drug-loaded biomedical materials, the drug should be stable in the polymer matrix during the storage period. The DSC thermograms of the membranes after storage for 1 month, 3 months, and 6 months (data not shown) showed that the thermal properties of the membranes did not change with storage time.

In the XRD pattern (Fig. 2C), the two diffraction peaks located at 21.4° and 23.8° are assigned to semi-crystalline PCL. The absence of a diffraction peak in the XRD pattern of gelatin indicates that gelatin is amorphous. As the MNA content increases, the two peaks of PCL shift to slightly higher angles, indicating that the length of PCL crystal stacks decreases, probably because the MNA molecules and gelatin molecular chains among the PCL molecular chains restrain the formation of PCL crystal stacks. The orientation of the PCL molecular chains during the electrospinning process also affects PCL crystallization. As the MNA content exceeds 10%, the characteristic diffraction peaks of MNA located at 12.2 °and 13.8 °appear, demonstrating the aggregation of MNA.

For bone/tissue regeneration, the porous membrane must be strong enough to withstand the forces during surgical operation and those exerted by physiological activities and/or by tissue growth [9]. The stress-strain curves in Fig. 2D show that the membranes are elastic, a property critical for GTR membranes. The tensile strengths of the membranes in the wet state are in the range of 3.8-8.6 MPa, which meet the clinical GTR requirements. With the increase of MNA content, the tensile strength first decreases, reaches a minimum at PGH10, which has the thinnest fibers, and then increases until PGH30.

3.1.4. Apparent WCA of the membranes

The hydrophilicity of biomaterials has great influence on the adhesion and proliferation of cells. The electrospun PGH-MNA membranes are all hydrophilic with contact angles of about 60° while PCL is moderately hydrophobic with a contact angle of 129.6°, as shown in Fig. 3. The incorporation of gelatin significantly increases the hydrophilicity of the membranes because of the amine and carboxyl functional groups in the gelatin structure. Besides, with the increase of MNA content, the contact angle decreases because of the hydroxyl and polar imidazole ring functional groups on the MNA molecule. Such an improvement in hydrophilicity will increase tissue regeneration and the biodegradation rate of the membranes.

3.1.5. Drug encapsulation efficiency and drug release profile of electrospun membranes

The drug encapsulation efficiencies of PGH1, PGH5, PGH10, PGH20, PGH30, and PGH40 which are 93.6%, 93.0%, 92.4%, 90.5%, 89.6%, and 87.1%, respectively, are higher than those of PG5, PG10, PG20, PG30, and PG40 which are 92.4%, 90.7%, 87.5%, 84.9, and 84.1%, respectively, because the better miscibility of PCL and gelatin results in better interaction of MNA with the polymer matrix and better dispersion of MNA in the nanofibers. With the increase of drug loading, the drug encapsulation efficiency decreases, probably because of the loss of a small part of the aggregated drug, which cannot be encapsulated into the nanofibers.

The drug release profiles of the PGH-MNA membranes are presented in Fig.4. About 40% of the MNA is released from the membranes within 1 day and 60% within 3 days, with an initial burst release. Then the MNA tends to release at a slower, linear rate until 3 weeks. The mechanism of drug release is based on drug diffusion and gelatin biodegradation. The MNA on the surface of the nanofibers burst releases to PBS. The interaction between MNA and the polymer matrix leads to a sustained release of MNA from the nanofibers after the burst release. The smaller the diameter of the fibers, the shorter the drug diffusion route and the faster the drug release. The biodegradation of gelatin is slowed by the entangled PCL chains. The crystallinity of PCL also affects the drug release profile. Under the effects of the above factors, the membranes show a controlled and sustained drug release.

3.1.6. In vitro biodegradation of electrospun membranes

A desirable feature of any implantable polymeric scaffold would be synchronization of polymer degradation with the replacement by natural tissue produced from cells [33]. The GTR membranes must function for at least 4–6 weeks to allow successful regeneration of the periodontal system [34]. The mass loss curves of different electrospun membranes are shown in Fig. 5A. In the first week, the mass loss of P30 is mainly due to MNA release while the mass loss of PGH30 is much higher than that of P30 because of the degradation of gelatin. The PGH-MNA nanofiber membranes show an obvious mass loss in 2 weeks caused by both drug release and gelatin hydrolysis on the surface of the nanofibers, followed by a slow and linear degradation because of the slow

hydrolysis of gelatin molecules inside the nanofibers and PCL molecules. The SEM micrographs of PGH30 15 days and 30 days after degradation show that the surface of the nanofibers becomes rough with a uniform degradation process. The degradation of gelatin molecular chains results in the increase of nanofibers surface roughness, therefore accelerating the infiltration of water into the nanofibers. Besides, the crystallinity of PCL decreases with the incorporation of HAc, so the degradation rates of the PGH-MNA membranes are accelerated. The uniform degradation process also indicates the entanglement of PCL and gelatin chains. After degradation for 3 months, 55%-70% by mass of the PGH-MNA membranes have degraded. As indicated in Fig.5B, after degradation for 1 month, the tensile strength of every membrane is sufficiently high to support the growth of new tissues.

3.2. Barrier function, in vitro antibacterial activity, and biocompatibility

3.2.1. Barrier function to fibroblast cells

The barrier function of the PGH-MNA nanofiber membranes were tested *in vitro* by simulating penetration of fibroblast cells into the membranes. As shown in Fig. S5, no cell gets to the opposite side of the membranes because the pores formed in the membranes are much smaller than fibroblast cells. All membranes after degradation for 1 month can still prevent the ingrowth of cells (data not shown).

3.2.2. In vitro antibacterial activity

Bacterial inhibition experiments were used to determine the minimal inhibition content of MNA loaded in the membranes. The growth of Fusobacterium nucleatum can be visualized directly from the plate (Fig. 6) to assess the antibacterial activity. Bacterial inhibition zones are clearly observed around the membranes. The membranes with MNA content over 5% show a more obvious antibacterial activity than PGH1 and can maintain long term antibacterial effects because of the slow but sustained release of MNA. Additionally, the membranes can inhibit bacterial growth in an area much larger than the membrane size because of the diffusion of MNA into the agar.

3.2.3. Cytotoxicity of PGH-MNA nanofiber membranes

According to the results of *in vitro* cytotoxicity (see S5), the PGH-MNA membranes show no cytotoxicity to L929 cells until the MNA content reaches 40%. Incubated in the extract substrates of the membranes, L929 cells show health growing morphologies. The membranes also show no cytotoxicity to hPDLFs and ROS cells.

3.2.4. Proliferation of cells on PGH-MNA nanofiber membranes

Attachment, adhesion, and spreading occur in the first phase of cell-material interactions and will influence the cell's capacity to proliferate on the biomaterial and cell morphology. The viability of the cells proliferated on the membranes indicates the biocompatibility of the membranes. For all the tested membranes, with incubation, the number of cells increases continuously during the 7 days of culture, as shown in Fig. 7A, indicating that all the membranes are nontoxic and support cell proliferation. For PGH40, as the MNA released in the culture medium reaches a sufficiently high content, the cell growth is adversely affected. As shown in Fig. 7B, hPDLFs and ROS cells also proliferate well after incubation for 48 hours on the membranes, with no statistical difference between the cells proliferating on the membranes and those proliferating on TCP as blank control. Because the antibacterial activities of PGH30 and PGH40 are higher those of other membranes but PGH40 adversely affects cell proliferation, a MNA content of 30% is the highest drug content with the best antibacterial activity but without cytotoxicity.

The morphology of L929 cells proliferating on PGH30 was observed by SEM and CLSM. Because the size of the cell is much larger than the pore size of membrane, the cells grow on the surface of the membrane without infiltrating in the thickness direction. As shown in both SEM and CLSM micrographs, after 3 days seeding, the L929 cells reach only approximately 30% confluency with most round shape. With proliferation, the number of cells increases significantly, forming almost a confluent layer with the characteristic spindle shape and stretching across the substrate on day 7. Cells demonstrate extension and spreading cytoskeleton from CLSM images. The specific structures—filopodia and lamellipodia—related to the cell motility of fibroblasts can be observed both

from SEM and CLSM micrographs. The cells emit cytoplasmic process towards the fibers and neighboring cells, communicating with the surrounding micro-environment and neighboring cells and allowing the passage of messengers [35]. Thus, we can conclude that even with a high content of drug and the use of organic solvent during the electrospinning process, PGH30 has no negative effect on cell morphology, viability, and proliferation.

3.3. In vivo biocompatibility and degradation of membranes

3.3.1. Gross morphology

From previous study, we have concluded that MNA-loaded PCL membrane is effective in reducing the inflammatory response after implantation (see S6). The effect of MNA content on the anti-inflammation ability and biocompatibility of the PGH-MNA nanofiber membranes was investigated. During the experiments, all the rabbits remained in good health with no wound complications. For all the membranes, no acute or chronic inflammation, necrosis, or adverse tissue reaction was identified. The membranes were absorbed completely after 6 months.

3.3.2. Histology

Host reactions following implantation of biomaterials include injury, blood-material interactions, provisional matrix formation, acute inflammation, chronic inflammation, granulation tissue development, foreign body reaction, and fibrous capsule development [36].

The 1 week post-operation is a high-incidence season of acute inflammatory response to biomaterials, which is marked by the presence of neutrophils. As shown in Fig. 8, at 1 week implantation, no neutrophils are observed around PGH5, PGH10, and PGH30, an indication of no obvious inflammatory response for these membranes. Fibroblasts infiltration on PGH10 and PGH30 are, on average, less than that on PGH5 at 1 week. At 3 weeks implantation, only a small amount of mononuclear cells were observed around the three membranes, showing no obvious chronic inflammation. Besides, the number of mononuclear cells around PGH5 is a little higher than that around PGH 10 and PGH30. No fibrous capsules form around the samples after 3 and 8 weeks implantation. At 8

weeks implantation, all three membranes start to degrade and the nanofibers break, resulting in increases in pore size and porosity. The biodegradation rate of PGH10 is higher than those of PGH5 and PGH30 because of the thinner nanofibers of PGH10. At week 12, fibroblasts have infiltrated into PGH5 and PGH10, but not PGH30. The surrounding tissues of all three membranes show a normal wound healing process. At 16 weeks implantation, a mass of fibroblasts, monocytes and multinucleated giant cells, as well as blood vessels are observed inside of PGH5 and PGH10. Most part of PGH5 and PGH10 are replaced by fibrous tissues. However, PGH30 still possess barrier function, and integration of PGH30 and fibrous tissue at the interface is achieved. At week 24, all three membranes are almost completely swallowed by macrophages.

3.3.3. In vivo degradation

In the design of GTR/GBR membrane, it is important to match the *in vivo* degradation rate of the membrane with the tissue regeneration rate [37]. The morphological changes of the nanofibers during *in vivo* degradation were evaluated by observing cross sections of the membranes by SEM (Fig. 9). After 16 weeks implantation, both PGH5 and PGH10 have degraded with nanofibers breakages, but PGH30 still retains the unique nanofiber morphology with no obvious fragmentation. The incorporation of gelatin increases the biodegradation rate of the membranes compared with P0 and P30, as shown in Fig. S7.

4. Discussion

The aim of the current study was to fabricate electrospun membranes with drug release as anti-infective GTR/GBR membranes and to evaluate their effects on bacterial growth, biocompatibility, and biodegradability. We hypothesized that an electrospun membrane loaded with antibacterial drug would reduce bacterial colonization and hence prevent infection which is considered as the major reason for GTR/GBR failure in clinical applications. For this purpose, different contents of MNA were loaded in PCL/gelatin nanofibers by using electrospinning.

To solve the immiscibility of natural gelatin and synthetic PCL, a tiny amount of HAc was introduced into the

electrospinning system. The phase separation of PCL and gelatin was solved, and the PCL and gelatin macromolecular chains were dispersed homogeneously in the uniform PGH-MNA nanofibers. Thus, the preparation of uniform and scalable production of the electrospun membranes was guaranteed. After the introduction of HAc, chains entanglement and strong interaction between PCL, gelatin, and MNA were formed. The mechanical properties and drug encapsulation efficiencies of the membranes were improved. Drug was released in a more controlled and sustained profile. The contact angles of PGH-MNA membranes were higher than those of PG-MNA membranes at the same MNA content. Gelatin nanofibers dispersed in a PG-MNA membrane increase the surface roughness of the membrane and absorb water, resulting in a decrease of contact angle. But with PCL and gelatin homogeneously dispersed in the nanofibers of a PGH-MNA membrane, the contact angle of the membrane is affected by the hydrophobic PCL and hydrophilic gelatin. Our experimental results indicated that electrospun PGH-MNA nanofiber membranes had improved properties over those of PG-MNA membranes, with a combination of the favorable biological properties of gelatin and mechanical properties of PCL. Because the electrospun PCL/gelatin membranes and other similar gelatin-based natural-synthetic hybrid systems are widely used in scaffolds, this approach may be broadly applied to achieve homogeneous hybrid nanofibers with improved properties.

Our main findings showed that PCL/gelatin electrospun nanofiber membranes acted as effective MNA carriers. The membranes showed appropriate mechanical properties and biodegradation rates. Cells could adhere and proliferate on the membranes without cytotoxicity until the MNA content reached 30%.The MNA released from the membranes effectively prevented the colonization of anaerobic bacteria. Electrospinning is an effective approach to functionalize PCL/gelatin membrane with MNA release. The membranes loaded with different contents of MNA showed a release profile independent of MNA content, including an approximately 60% release of MNA within 1 week, followed by a sustained release of up to 3 weeks. Such a release profile was predominantly

controlled by diffusion and gelatin degradation. A large burst release is often regarded as a negative consequence for certain long term controlled release materials. However, in our case for anti-infective drug delivery, when a material is implanted into a tissue defect site, the first week is the high-incidence season of infection and inflammation. So a high initial release rate in the first few days after the implant is best for eliminating the intruding bacteria that are introduced during the implantation and systemically afterwards before they begin to proliferate. For the few bacteria that may survive the initial burst, a continued drug release is necessary to prevent their further population and inhibit the occurrence of latent infection [38]. So this 3-week prolonged drug release is considered to be an optimal treatment. Besides, the clinically recommended oral dosage of MNA for an adult patient is 0.4 g-0.8 g every time, which is much larger than the minimal inhibitory concentration value (0.2-2 mg/L) used to inhibit the growth of anaerobic bacterial. According to the density of the electrospun membranes (~0.36 g/cm^3) and the prototypical mediated dimension of a GTR membrane (5 cmx5 cmx250 μm), the total amount of MNA in PGH30 is about 0.047 g. The concentration of drug released at the tissue defect site in the first week is sufficiently high to inhibit the growth of bacteria, but much lower than the systemic treatment dosage.

The *in vivo* experiments demonstrated that the organic solvent used in the electrospinning process had no adverse effect on the biocompatibility of the membranes. The membranes had good barrier function, as shown by the *in vitro* experiments, which could be used to effectively predict the *in vivo* barrier function of the membranes, so animal experiments could be avoided. PGH-MNA membranes were effective in reducing the inflammatory response after implantation, and all possessed good biocompatibility. The membranes showed different biodegradation rates with different MNA contents. Thus, we could choose the MNA content loaded in the nanofiber membranes depending on the level of infection and biodegradation time required of the regenerating tissue.

5. Conclusions

We developed an efficient, anti-infective GTR/GBR membrane made by metronidazole-loaded electrospun PCL/gelatin nanofibers. The phase separation of immiscible PCL and gelatin was mediated by introducing a tiny amount of HAc. A wide range of drugs (1-40 wt.%) were successfully incorporated into and released from the membranes. The MNA-loaded membranes can reduce inflammatory response upon implantation in rabbits by delivering MNA locally. PGH30 showed excellent comprehensive properties both *in vitro* and *in vivo*. Hence, PGH30 can be an optimal choice for localized drug delivery GTR/GBR membrane for the prevention of implant-associated infection. Besides, this drug delivery membrane can be used in various therapeutic applications in which controlled drug delivery is necessary, including pathologies demanding chronic drug treatments, wound healing, prevention of post-surgical adhesions and tissue engineering applications.

Acknowledgements

This work was supported by the National Natural Science Foundation of China (50933001, 51221102, 81171682, and 81330043), Beijing Nova Program (Z131102000413015), and the RCUK China-UK Science Bridges Program through the Medical Research Council and the Engineering and Physical Sciences Research Council.

References

[1] Karring T, Nyman S, Lindhe J. Healing following implantation of periodontitis affected roots into bone tissue. J Clin Periodontol 1980;7:96-105.

[2] Gentile P, Chiono V, Tonda-Turo C, Ferreira AM, Ciardelli G. Polymeric membranes for guided bone regeneration. Biotechnol J 2011;6:1187-97.

[3] Retzepi M, Donos N. Guided Bone Regeneration: biological principle and therapeutic applications. Clin Oral Implants Res 2010;21:567-76.

[4] Vasilev K, Cook J, Griesser HJ. Antibacterial surfaces for biomedical devices. Expert Rev Med Devices 2009;6:553-67.

[5] Campoccia D, Montanaro L, Arciola CR. A review of the biomaterials technologies for infection-resistant surfaces. Biomaterials 2013;34:8533-54.

[6] Campoccia D, Montanaro L, Arciola CR. A review of the clinical implications of anti-infective biomaterials and infection-resistant surfaces. Biomaterials 2013;34:8018-29.

[7] Feng K, Sun H, Bradley MA, Dupler EJ, Giannobile WV, Ma PX. Novel antibacterial nanofibrous PLLA scaffolds. J Control Release 2010;146:363-9.

[8] Vacanti NM, Cheng H, Hill PS, Guerreiro JoD, Dang TT, Ma M, et al. Localized delivery of dexamethasone from electrospun fibers reduces the foreign body response. Biomacromolecules 2012;13:3031-8.
[9] Bottino MC, Thomas V, Schmidt G, Vohra YK, Chu TM, Kowolik MJ, et al. Recent advances in the development of GTR/GBR membranes for periodontal regeneration--a materials perspective. Dent Mater 2012;28:703-21.
[10] Loesche WJ. Role of anaerobic bacteria in periodontal disease. Ann Otol Rhinol Laryngol Suppl 1991;154:43-5.
[11] Freeman CD, Klutman NE, Lamp KC. Metronidazole. A therapeutic review and update. Drugs 1997;54:679-708.
[12] Löfmark S, Edlund C, Nord CE. Metronidazole is still the drug of choice for treatment of anaerobic infections. Clin Infect Dis 2010;50:S16-S23.
[13] Kurtis B, Ünsal B, Çetiner D, Gültekin E, Özcan G, Çelebi N, et al. Effect of polylactide/glycolide (PLGA) membranes loaded with metronidazole on periodontal regeneration following guided tissue regeneration in dogs. J Periodontol 2002;73:694-700.
[14] Hu C, Cui W. Hierarchical Structure of Electrospun Composite Fibers for Long-Term Controlled Drug Release Carriers. Adv Healthc Mater 2012;1:809-14.
[15] Qiu K, He C, Feng W, Wang W, Zhou X, Yin Z, et al. Doxorubicin-loaded electrospun poly (L-lactic acid)/mesoporous silica nanoparticles composite nanofibers for potential postsurgical cancer treatment. J Mater Chem B 2013;1:4601-11.
[16] Zeng J, Yang L, Liang Q, Zhang X, Guan H, Xu X, et al. Influence of the drug compatibility with polymer solution on the release kinetics of electrospun fiber formulation. J Control Release 2005;105:43-51.
[17] Shields KJ, Beckman MJ, Bowlin GL, Wayne JS. Mechanical properties and cellular proliferation of electrospun collagen type II. Tissue Eng 2004;10:1510-7.
[18] Bergsma J, De Bruijn W, Rozema F, Bos R, Boering G. Late degradation tissue response to poly (L-lactide) bone plates and screws. Biomaterials 1995;16:25-31.
[19] Reichert JC, Cipitria A, Epari DR, Saifzadeh S, Krishnakanth P, Berner A, et al. A tissue engineering solution for segmental defect regeneration in load-bearing long bones. Sci Transl Med 2012;4:141ra93.
[20] Dash TK, Konkimalla VB. Poly-ϵ-caprolactone based formulations for drug delivery and tissue engineering: A review. J Control Release 2012;158:15-33.
[21] Ma Z, He W, Yong T, Ramakrishna S. Grafting of gelatin on electrospun poly (caprolactone) nanofibers to improve endothelial cell spreading and proliferation and to control cell orientation. Tissue Eng 2005;11:1149-58.
[22] Gupta D, Venugopal J, Prabhakaran MP, Dev V, Low S, Choon AT, et al. Aligned and random nanofibrous substrate for the in vitro culture of Schwann cells for neural tissue engineering. Acta Biomater 2009;5:2560-9.
[23] Xue J, Feng B, Zheng R, Lu Y, Zhou G, Liu W, et al. Engineering ear-shaped cartilage using electrospun fibrous membranes of gelatin/polycaprolactone. Biomaterials 2013;34:2624-31.
[24] Zheng R, Duan H, Xue J, Liu Y, Feng B, Zhao S, et al. The influence of Gelatin/PCL ratio and 3-D construct shape of electrospun membranes on cartilage regeneration. Biomaterials 2014;35:152-64.
[25] Ji W, Yang F, Ma J, Bouma MJ, Boerman OC, Chen Z, et al. Incorporation of stromal cell-derived factor-1α in PCL/gelatin electrospun membranes for guided bone regeneration. Biomaterials 2013;34:735-45.
[26] Feng B, Tu H, Yuan H, Peng H, Zhang Y. Acetic-acid-mediated miscibility toward electrospinning homogeneous composite nanofibers of GT/PCL. Biomacromolecules 2012;13:3917-25.
[27] Chong EJ, Phan TT, Lim IJ, Zhang YZ, Bay BH, Ramakrishna S, et al. Evaluation of electrospun PCL/gelatin nanofibrous scaffold for wound healing and layered dermal reconstitution. Acta Biomater 2007;3:321-30.
[28] Signat B, Roques C, Poulet P, Duffaut D. Fusobacterium nucleatum in periodontal health and disease. Curr

Issues Mol Biol 2011;13:25-36.
[29] Boyle VJ, Fancher ME, Ross RW, Jr. Rapid, modified Kirby-Bauer susceptibility test with single, high-concentration antimicrobial disks. Antimicrob Agents Chemother 1973;3:418-24.
[30] Amin S, Shetty HK, Varma RK, Amin V, Nair PM. Comparative evaluation of antibacterial activity of total-etch and self-etch adhesive systems: An ex vitro study. J Conserv Dent 2014;17:266-70.
[31] Kim MS, Jun I, Shin YM, Jang W, Kim SI, Shin H. The development of genipin-crosslinked poly(caprolactone) (PCL)/gelatin nanofibers for tissue engineering applications. Macromol Biosci 2010;10:91-100.
[32] Meng Z, Zheng W, Li L, Zheng Y. Fabrication and characterization of three-dimensional nanofiber membrance of PCL–MWCNTs by electrospinning. Mater Sci Eng C Mater Biol Appl 2010;30:1014-21.
[33] Hutmacher DW. Scaffolds in tissue engineering bone and cartilage. Biomaterials 2000;21:2529-43.
[34] Sculean A, Nikolidakis D, Schwarz F. Regeneration of periodontal tissues: combinations of barrier membranes and grafting materials–biological foundation and preclinical evidence: a systematic review. J Clin Periodontol 2008;35:106-16.
[35] Ji W, Yang F, Seyednejad H, Chen Z, Hennink WE, Anderson JM, et al. Biocompatibility and degradation characteristics of PLGA-based electrospun nanofibrous scaffolds with nanoapatite incorporation. Biomaterials 2012;33:6604-14.
[36] Anderson JM, Rodriguez A, Chang DT. Foreign body reaction to biomaterials. Semin Immunol; 2008; 86-100.
[37] Thibault RA, Mikos AG, Kasper FK. Scaffold/Extracellular Matrix Hybrid Constructs for Bone-Tissue Engineering. Adv Healthc Mater 2013;2:13-24.
[38] Kim K, Luu YK, Chang C, Fang D, Hsiao BS, Chu B, et al. Incorporation and controlled release of a hydrophilic antibiotic using poly (lactide-co-glycolide)-based electrospun nanofibrous scaffolds. J Control Release 2004;98:47-56.

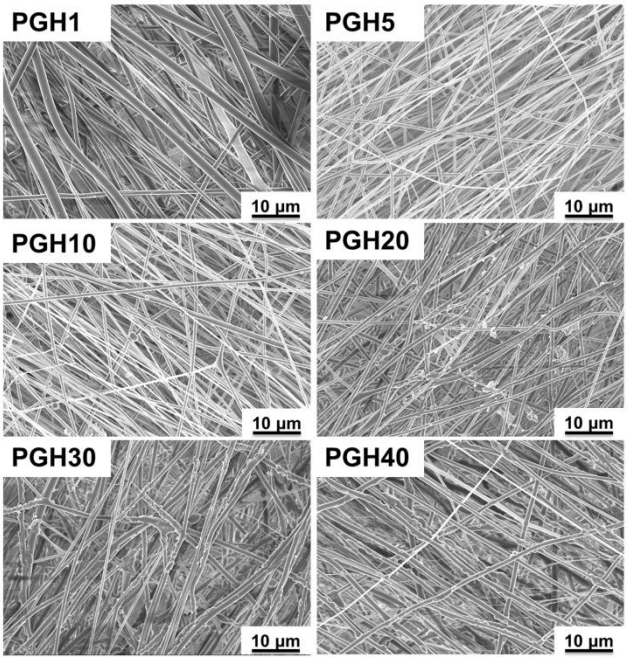

Fig. 1. SEM micrographs of electrospun nanofiber membranes with different contents of MNA.At low drug contents, the surface of the nanofibers is smooth. As the MNA content increases to 20%, a small amount of nanoparticles appear and are embedded on the surface of the nanofibers, demonstrating the formation of drug crystals.

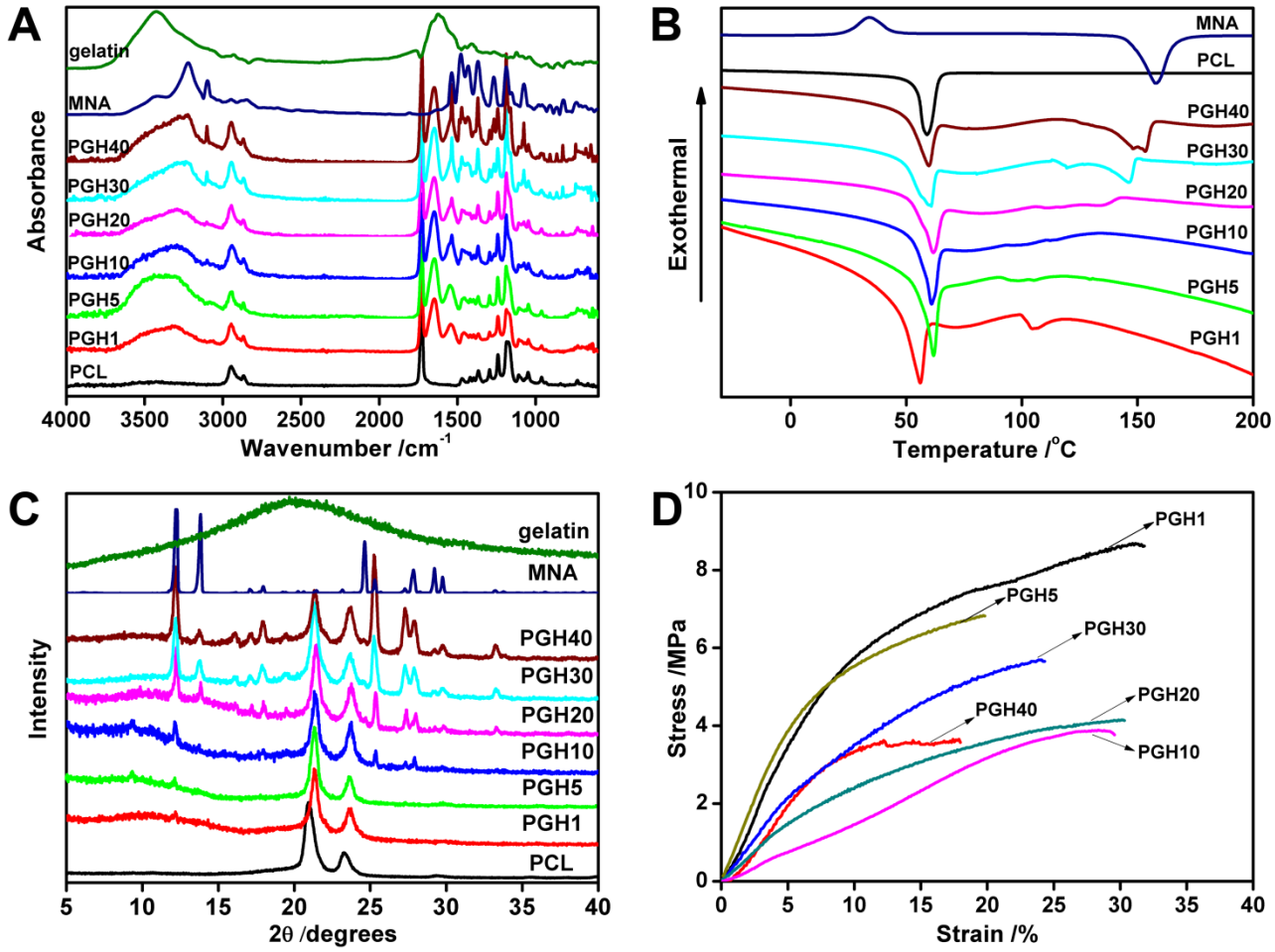

Fig. 2. Chemical, thermal, and mechanical properties of the electrospun membranes: (A) FTIR spectra, (B) DSC thermograms, (C) XRD patterns, and (D) stress-strain curves in the wet state.

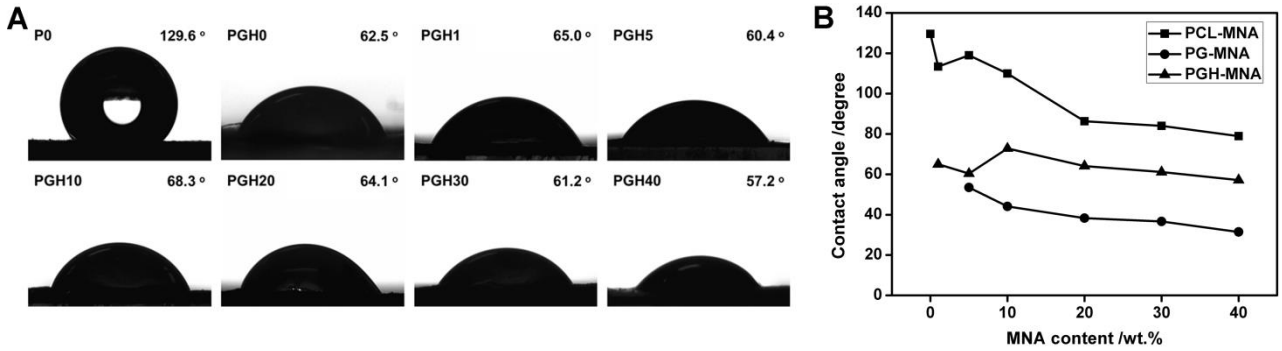

Fig. 3. (A) Water drop on the surface of the membranes and (B) the water contact angles of the membranes with different polymer matrix and MNA content.

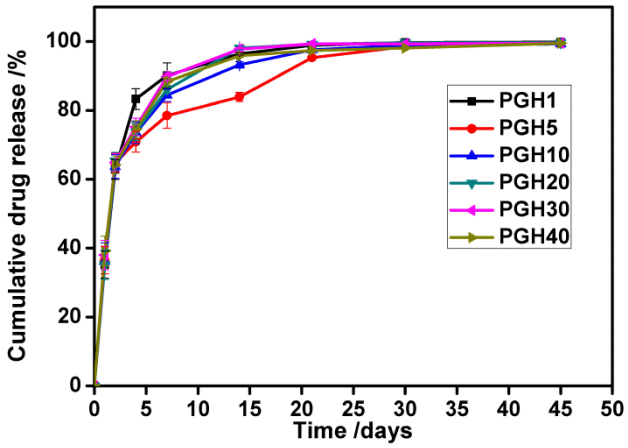

Fig. 4. Cumulative drug release profiles of the electrospun membranes at different soaking times in PBS.

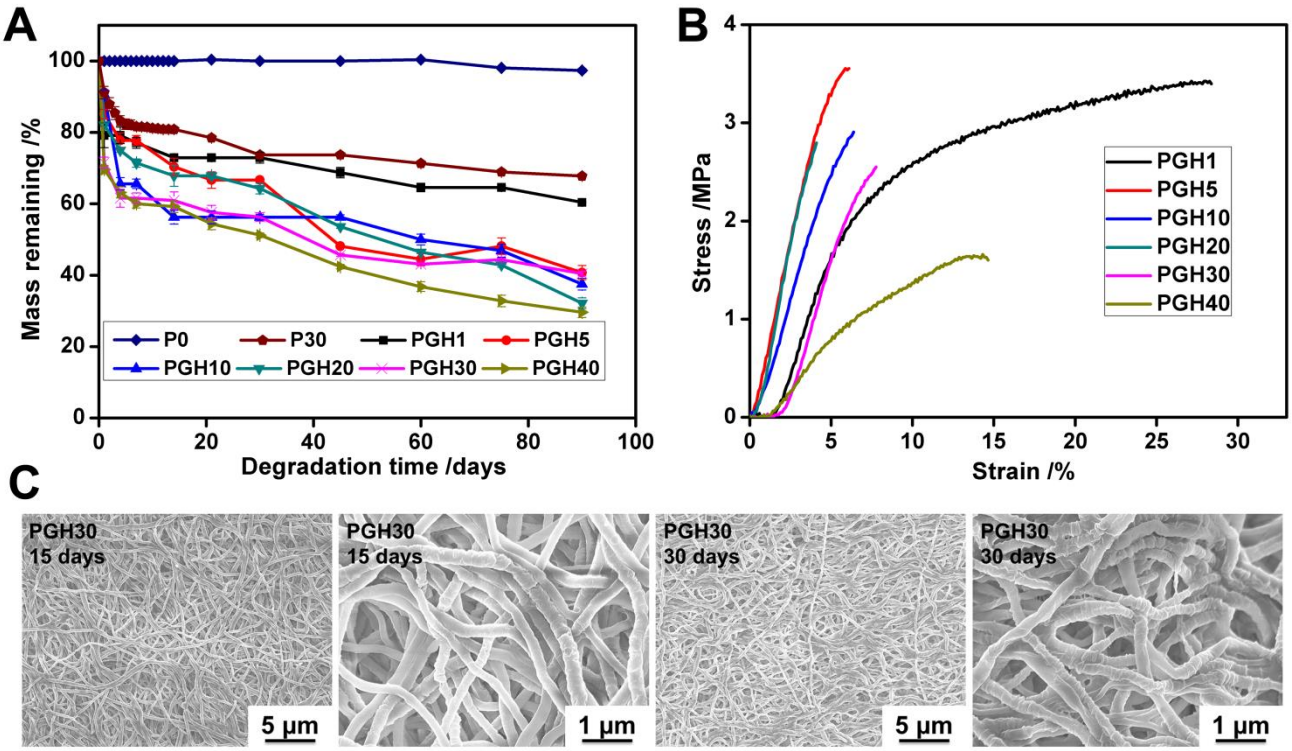

Fig. 5. *In vitro* degradation of electrospun membranes: (A) mass loss during 3 months degradation, and (B) stress-strain curves and (C) SEM micrographs of PGH30 after degradation for 15 days and 30 days in PBS.

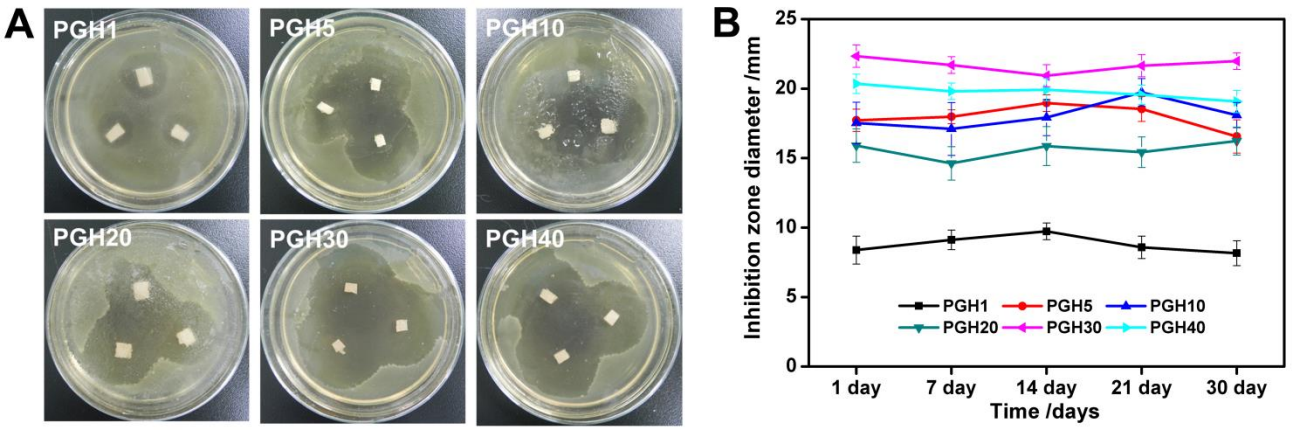

Fig. 6. Inhibition of bacterial growth on agar plates: (A) inhibition zone surrounding membranes with different contents of MNA after incubation for 1 day under anaerobic conditions at 37 ºC; (b) inhibition zone diameter versus incubation time for membranes with different drug contents.

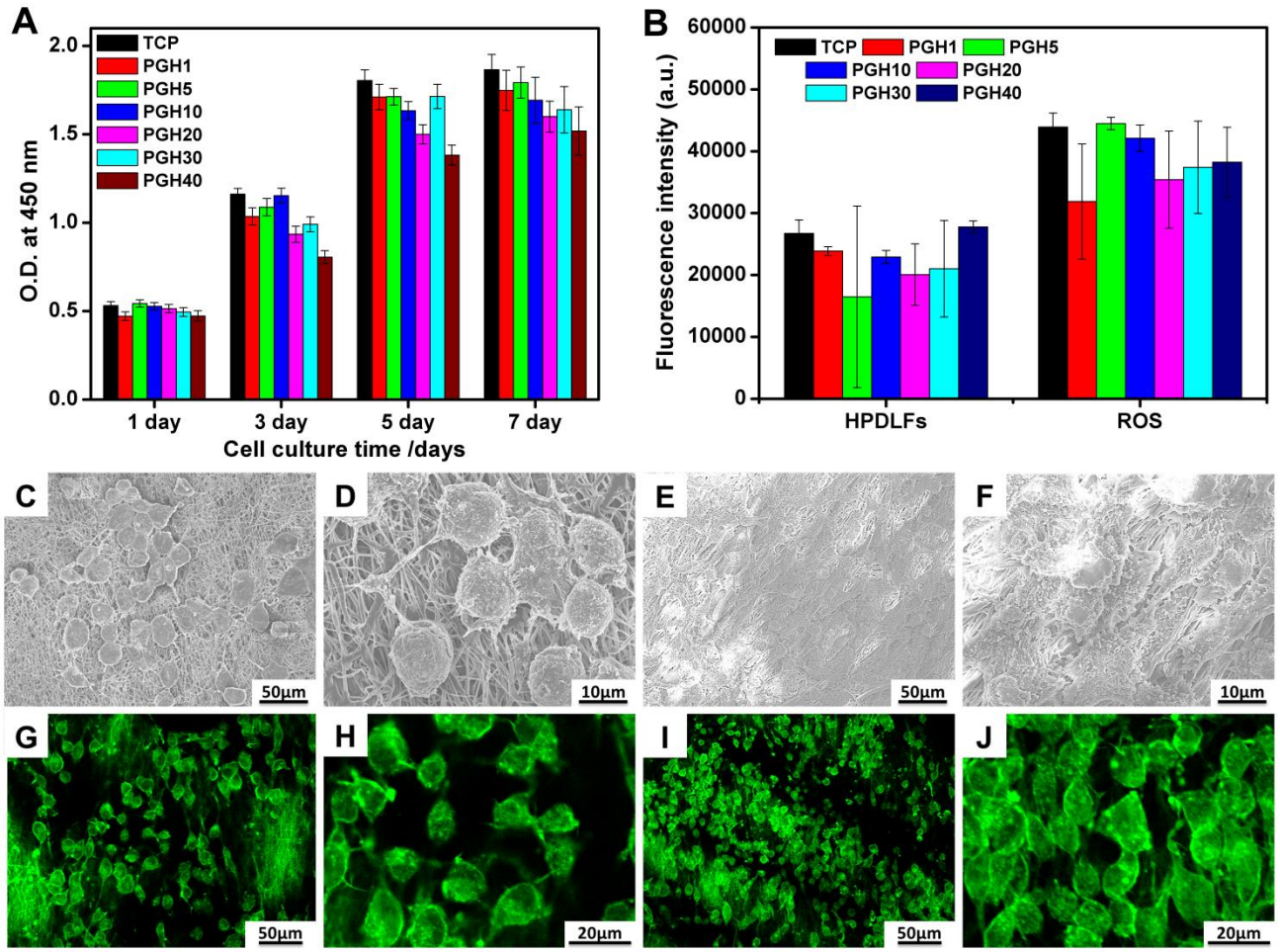

Fig. 7. Viability of cells proliferated on the membranes: (A) optical density (O.D.) of L929 cells proliferated 1, 3, 5, and 7 days and (B) fluorescence intensities of hPDLFs and ROS cells cultured for 48 hours. SEM micrographs and

confocal fluorescent images of L929 cells proliferated on PGH30 for (C)(D)(G)(H) 3days and (E)(F)(I)(J) 7 days.

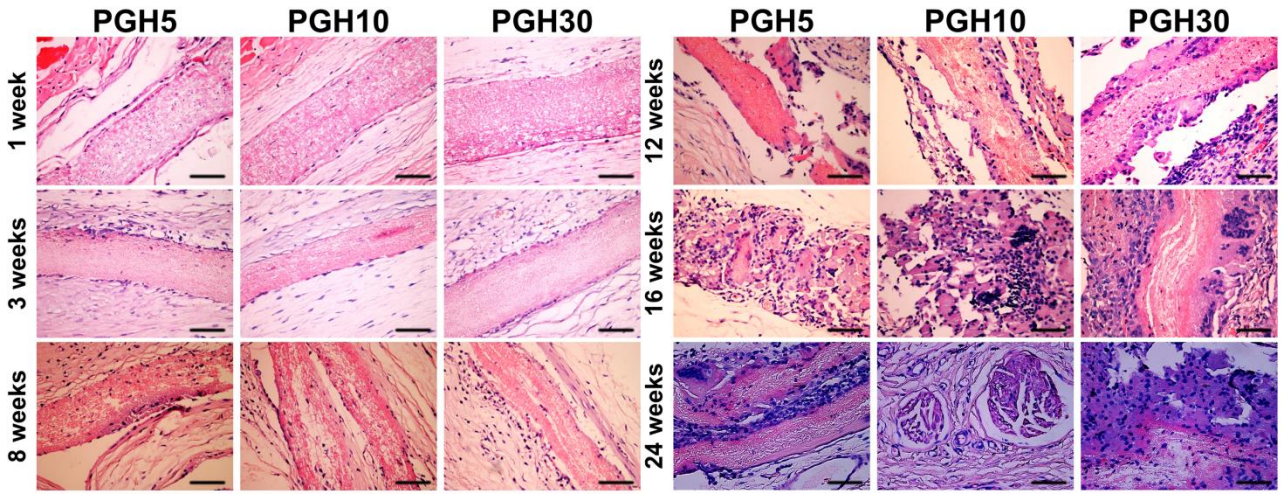

Fig. 8. Histological micrographs of PGH5, PGH10 and PGH30 with H&E staining (scale bar = 100 μm).

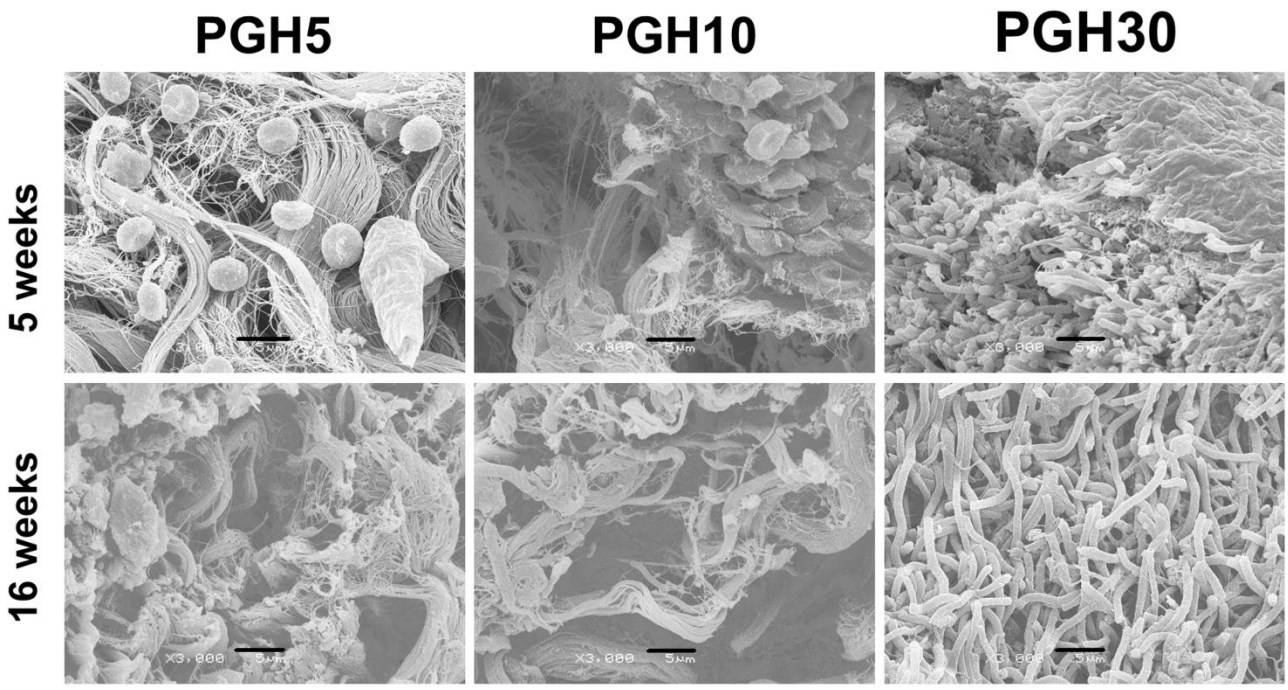

Fig. 9. SEM micrographs of longitudinal sections of membranes at different time after subcutaneous implantation (scale bar = 5 μm).

Table 1. Fiber diameter, pore size,and porosity of electrospun membranes with different contents of MNA

Sample	MNA (w/w%)	Fiber diameter (μm)	Pore size(μm)	Apparent density (g/cm^3)	Porosity (%)
PGH1	1	1.10±0.20	3.2±0.7	0.34	71.7
PGH5	5	1.34±0.30	4.3±1.3	0.37	69.5
PGH10	10	0.43±0.10	2.8±0.4	0.33	72.3
PGH20	20	0.59±0.10	3.3±0.7	0.35	71.2
PGH30	30	0.97±0.20	4.0±0.7	0.35	70.9
PGH40	40	1.02±0.40	4.2±1.1	0.37	69.2